Direct simulations of aggregates in homogeneous isotropic turbulence

J.J. Derksen

Chemical & Materials Engineering, University of Alberta, Edmonton, Alberta, T6G 2G6 Canada,

jos@ualberta.ca

Submitted to Acta Mechanica

Special Issue on Anisotropic Particles in Turbulent Flows, Oct. 2012

Revision submitted: February 2013

2nd revision submitted: April 2013

Accepted April 2013

Abstract

We study aggregation in turbulent flow by means of particle-resolved, direct numerical simulations (DNS). Mono-sized spheres with an attractive square-well potential are released in homogeneous, isotropic turbulence generated through linear forcing. Typical cases have a solids volume fraction of 0.08 and a ratio of the Kolmogorov scale over the primary sphere radius of O(0.1). The latter implies that the flow around the primary spheres is inhomogeneous. The simulations show the continuous formation and breakage of aggregates as a result of the turbulence and the attractive potential. The average size of the aggregates is a pronounced function of the strengths of turbulence and interaction potential. Fractal dimensions of the aggregates are in the range 1.4 to 1.8 for the cases studied.

1 Introduction

If sticky particles are suspended in a turbulent flow, turbulence plays a dual role in the evolution towards a (dynamically) steady aggregate size distribution. On one side, the turbulence promotes collisions between particles due to its relative velocities, and a collision is a necessary first step in an aggregation event. On the other side the turbulence provides a means for aggregate breakage due to the stresses imposed by the flow on the aggregate. A second mechanism of aggregate breakage is collisions between aggregates and/or primary particles that potentially destabilize aggregates. Based on the above sketch, the aggregate size distribution is expected to be a function of turbulence properties (intensity of turbulence and the length scales of turbulence relative to particle sizes), solids properties (including solid over liquid density ratios and solids volume fraction) and the properties of the attractive interaction potential between the particles that is responsible for aggregation.

This paper focuses on simulations of aggregation in turbulence with two specific, atypical characteristics. In the first place we consider the primary spherical particles (that all have the same radius a) to be larger than the Kolmogorov length scale η_K of the turbulent flow (here η_K/a is in the range 0.1 to 0.4). In the second place we only consider reversible aggregation: the formation and breakage of bonds between particles conserve energy and the bonds are non-rigid. A consequence of the first characteristic is that the flow around individual primary particles and around aggregates is inhomogeneous with more than one turbulent microstructure interacting with a particle simultaneously. This makes it desirable to resolve the flow on scales smaller than the size of primary particles so as to capture accurately the solid-turbulence interactions and thus the particle dynamics. Non-rigid and reversible bonds imply that aggregates continuously restructure, break, and bond so that the aggregate size distribution (ASD) and aggregate morphology are dynamic entities. In the simulations we aim at reaching a dynamic steady state and subsequent characterization of the particle and fluid dynamics in this steady state.

The intention of fully resolving the flow and particle dynamics, along with the specific characteristics of our aggregating systems (see above) distinguishes this research from the large body of

literature on simulations of aggregation processes involving solid particles suspended in liquids. Resolution at the length scale of the primary particles and computational feasibility also implies that we have to limit the size of the domain that is simulated. At the same time, the domains have to be sufficiently large to develop and sustain turbulence with its wide spectrum of length scales. We have been using fully periodic, three-dimensional domains and forced turbulence for this. The simulations then mimic a homogeneous, meso-scale portion of an aggregation reactor, away from walls and turbulence generating devices (such as impellers).

A significant portion of the literature on aggregation deals with population balance equations (PBEs) where the processes of aggregate formation and breakage are parameterized with "kernels" that are functions of (local) flow characteristics, solid and liquid properties, and the details of the interparticle interactions (bond strengths, particle surface properties etc.) [1]. Developments in the field of PBEs relate to solution strategies, such as methods based on the moments of ASDs [2] and the method of characteristics [3], and on the identification of the mathematical structure of aggregation and breakage kernels that allow for ASDs to reach a dynamic equilibrium [4]. The predictive power of PBE solutions critically depends on the physics contained in the breakage and aggregation kernels.

Detailed simulations of aggregates, aggregation, restructuring, and breakage reported in the literature are restricted to solid-liquid suspensions undergoing homogeneous deformations [5-12]. This is a valid approach to be applied for turbulent systems containing particles much smaller than the Kolmogorov scale and generally allows for a Stokes flow approximation at the scale of the particles.

The methodology used in this paper has been described in detail previously [13] and we limit ourselves to a short summary. Homogeneous, isotropic turbulence (HIT) is generated and sustained in a cubic, fully periodic, three-dimensional domain with side length of 32 to 64 times a through linear forcing [14]. With linear forcing we have control over the energy dissipation rate (and thus the Kolmogorov length scale) once stationary conditions are reached and dissipation balances power input. In the turbulent field, uniformly sized, spherical primary particles are released. The solids typically occupy 8% of the total

volume. The particles have a tendency to aggregate by means of a square-well potential defined by a distance of interaction δ, and a binding energy E_{swp} [15]. As indicated above, this is a reversible interaction. If the centers of two approaching spheres come within a distance $2(a+\delta)$ they exchange potential energy for kinetic energy (by an amount E_{swp} per sphere). Two attached spheres can only separate if they are able to overcome the potential energy barrier imposed by the square-well potential with their kinetic energy. If they separate, kinetic energy is converted back into potential energy.

The simulations are based on the lattice-Boltzmann method for simulating fluid flow [16,17]. The no-slip conditions at the moving sphere surfaces are imposed through an immersed boundary method [18,19]. By applying the immersed boundary method on each sphere surface we resolve the solid-liquid interfaces and the hydrodynamic force and torque acting on each sphere. These we use to update the spheres' linear and rotational equations of motion. This directly couples the solids and fluid phase, and fully accounts for the finite size of the particles.

The present paper builds on the previous paper [13] in that it extends the range of parameters studied (specifically the range of η_K/a), and that it explores the consequences of agglomeration for the dynamics of the primary solid spheres. The paper is organized in the following manner: we first define the flow systems in terms of dimensionless numbers. We then briefly discuss the numerical procedure. We show results for aggregation in homogeneous, isotropic turbulence with emphasis on aggregate size distributions, aggregate fractal dimension, and solids velocity distribution functions as a function of flow and particle properties. At the end of the paper we summarize and draw conclusions.

2 Flow systems

The simulation domains are fully periodic cubes, of volume L^3 that contain an incompressible Newtonian fluid (density ρ and kinematic viscosity ν), and uniformly sized solid spherical particles with radius a and density ρ_p. The solids volume fraction ϕ has been fixed in this paper to 0.08; the aspect ratio L/a is

the range $42\frac{2}{3}$ to 64. Previous work [13] showed that for the typical conditions considered a domain size of $L \geq 32a$ is required to obtain results (e.g. in terms of the aggregate size distribution) that are not sensitive to the size of the domain. The density ratio ρ_p / ρ is 4.0 in all cases.

In the flow domain we create homogeneous, isotropic turbulence through linear forcing [14]. Linear forcing allows for sustaining turbulence with a pre-defined energy dissipation rate ε in single, as well as in multiphase (solid-liquid) flow [13]. Controlling ε implies that we also control the Kolmogorov length-scale $\eta_K = \left(\frac{\nu^3}{\varepsilon} \right)^{1/4}$, and η_K / a is a dimensionless input parameter to the simulations. The solid spheres suspended in the turbulent flow interact via a square-well potential [13,15] that serves as the model mechanism for aggregation. The square well is defined by the two parameters δ and Δu that characterize its reach and strength respectively. Two approaching spheres that come within a center-to-center distance $2(a+\delta)$ attach and exchange potential energy for kinetic energy. If two attached spheres separate they need a relative velocity along the line connecting the two sphere centers of at least $2\Delta u$ to detach. This implies [13] that the square well has a depth of $E_{swp} = \frac{1}{2} m_p (\Delta u)^2$ with $m_p = \frac{4}{3} \pi \rho_p a^3$ the mass of the primary spheres. Attached spheres keep moving under the influence of hydrodynamic forces (non-rigid bonds) and possibly undergo hard-sphere collisions. For collisions we use the two parameter model due to Yamamoto et al [20] that has a restitution coefficient *e* and friction coefficient μ. In many of the simulations in this paper the friction coefficient μ was set to infinity which means that in such a simulation in a collision the two spheres attain the same surface velocity at their point of contact (note that since the particles are allowed to rotate, the surface velocity has a translational and a rotational contribution).

We thus have four parameters governing direct (as opposed to hydrodynamic) particle-particle interactions. In dimensionless form these are the collision parameters *e* and μ, and the square-well parameters δ / a, and $\Delta u / \upsilon$ with $\upsilon = (\nu \varepsilon)^{1/4}$ the Kolmogorov velocity scale. We keep the restitution

coefficient constant and equal to e=1.0 and fix δ/a to 0.05; for μ we have taken the two extremes μ=0 (smooth sphere surfaces) and $\mu \to \infty$ (sticking collisions, see above). In this paper $\Delta u/\upsilon$ equals 0.30. The choice for δ/a=0.05 implies a rather long-range interaction. With Kolmogorov scales in the micrometer range for strong turbulence, also a will be of that order. This makes that δ is of the order of 100 nm, typically larger than the reach of Van der Waals forces (order 10 nm).

3 Modeling approach

As in our previous works on direct simulations of liquid-solid suspensions with full resolution of the interfaces, we used the lattice-Boltzmann (LB) method [16,17] to solve for the flow of the interstitial liquid combined with an immersed boundary method to deal with the no-slip condition at the surfaces of the (translating and rotating) spherical particles [17,18]. The specific LB scheme employed here is due to Somers [21]. The immersed boundary method provides the hydrodynamic force and torque acting on each sphere. These are subsequently used to update the linear and rotational equations of motion of each particle. The simulations presented in this paper all have a resolution such that $a = 6\Delta$ with Δ the spacing of the uniform, cubic lattice used in the LB method. The choice for this resolution is based on earlier papers [22,23] where we compared numerical results with experimental data and performed grid refinement studies. Once the spatial resolution is fixed, the temporal resolution of the LB simulations goes via the choice of the kinematic viscosity. In all simulations discussed here the viscous time scale a^2/ν corresponds to 7200 time steps.

If the distance between sphere surfaces gets smaller than Δ, the LB flow solver does not resolve the flow dynamics between the spheres anymore. To deal with these short range hydrodynamic interactions we determine the radial lubrication force between the spheres (based on Stokes flow in the gap between the spheres [24]) that depends on the separation distance, the relative velocity, a and ν. A smooth way to switch on lubrication, and to saturate lubrication at very small separation has been described in detail in [22].

The spheres' equations of linear and rotational motion including resolved and unresolved (i.e. lubrication) forces are integrated according to an Euler forward method. These time-step driven updates are linked with an event-driven algorithm that detects events related to hard-sphere collisions, and attachment and detachment of spheres. Once an event is detected, all particles are frozen and the event is carried out which generally implies an update of the linear and angular velocities of the two spheres involved in the event. Subsequently all spheres continue moving until the end of the time step, or until the next event, whichever comes first.

4 Results

As compared to our previous paper on aggregation [13], two specific topics are further explored in the present paper. In the first place we observe the aggregation process from the perspective of individual primary particles. Issues that are considered from this perspective are the size of the aggregates the primary spheres are part of and on what time scales this fluctuates; and how the primary particle velocities (and velocity fluctuations) relate to the aggregation process. In the second place the effect of the strength of the turbulence (as a metric for this we use the volume-averaged power input and via this the ratio η_K/a) on the ASD (including the average aggregate size), and on the fractal dimensions of the aggregates has been investigated. Compared to reference [13] the η_K/a-range has been significantly extended. The base-case we refer to below is characterized by the dimensionless numbers given in Table 1.

Impressions of the simulations, and the aggregates formed are given in Figure 1. In the base-case the number of primary particles is 4995 and it is not very instructive to look at all particles in the volume (as we do in Figure 1A). The fact that we do simulations, however, allows us to visualize the multiphase system in (virtually) any conceivable manner. In Figure 1B the four largest aggregates (an aggregate is defined as group of attached spheres) are displayed; it shows open aggregate structures and it emphasises the periodic conditions given that the red aggregate is connected through the side boundaries. In Figure

1C the particles forming the largest aggregate identified in 1B ($n_{agg} = 150$) are followed in time. Defining t=0 as the moment the snapshots 1A and 1B were taken we go back in time $4\tau_K$, and ahead in time by the same amount. This shows that (re) structuring, "breakage" and aggregation are processes that take place on time scales comparable to τ_K . This observation is consistent with the time series in Figure 2. For this figure we randomly selected three primary particles and followed them in time. In the middle panel the size of the aggregate they are part of is displayed. This is a highly intermittent quantity that also shows that the lifetime of large aggregates is mostly very short but in some cases can extend over order 10 Kolmogorov times. In the top panel of Figure 2 the speed of the same primary spheres is tracked. The time scales of speed fluctuations are comparable to those of aggregate size.

A closer look at Figure 2 and relating its top two panels (as we do in the bottom panel) reveals a correlation between aggregate size and velocity: When a primary sphere is part of a larger aggregate is tends to move slower which would make sense given the increased solids inertia in the direct environment of the primary sphere. To investigate this further and with enhanced statistical significance, velocity probability distribution functions (pdf's) of primary spheres have been determined (based on all particles and longer time series as compared to the data in Figure 2), see Figure 3. Instead of aggregate size, we distinguish between primary spheres by means of the number of primary spheres they are in contact with (symbol n_c). Spheres are attached to up to 7 neighbouring spheres simultaneously. There is a clear correlation between n_c and aggregate size, see Figure 4. We indeed see a shift of the pdf's towards lower velocities if a sphere has many spheres attached to it. The pdf's for the higher n_c (4 and 6) as displayed in the left panel of Figure 3 are noisy because they are based on a limited number of occurrences. The shift of the pdf's towards lower speeds is further visualized by plotting the widths of the distributions as a function of n_c in the right panel of Figure 3.

We now turn to ASDs and their dependence on flow conditions and solids properties. To start with the latter, Figure 5 shows that seemingly minor detail such as the friction between primary spheres upon

colliding has a significant impact on the ASD with on average much smaller aggregates for smooth ($\mu = 0$) collisions. Note that the collisions in the two cases in Figure 5 have restitution coefficient e=1. If $\mu \neq 0$, however, much linear momentum is converted into angular momentum and since escape from the square-well potential is based on kinetic energy contained in translation (not rotation), frictional collisions lead (on average) to larger aggregates.

Potentially more relevant is the effect of changing the energy input – and thus the dissipation – on the formation of aggregates. In non-dimensional terms we look at the effect of the Kolmogorov size relative to the primary sphere radius (η_K / a) on the ASD. The results are summarized in Figure 6. Two domain sizes have been used to study this effect: L=256 and L=384. To generate representative turbulence including a sufficiently developed cascade that transfers energy from large to small (dissipative) scales a sufficiently large ratio L/η_K is required; typically $L/\eta_K \geq 100$. Since the sphere radius is fixed to 6Δ (to resolve the flow at the particle scale), increasing the ratio η_K / a requires increasing the domain size L. The largest η_K / a we investigated was 0.36 which implies $\eta_K \approx 2\Delta$ and for this simulation we deemed L=384 appropriate. A disadvantage of these large domains is that – given finite computational resources – we cannot run the simulations over very long times which somewhat limits the quality of the statistics of the results. The trends in Figure 6 are, however, clear. Larger aggregates form if η_K / a gets larger. That an increase in η_K / a, and thus a decrease in the dissipation rate indeed implies weaker turbulence is shown in Figure 7 where the root-mean-square velocity in the liquid phase is plotted against η_K / a. Average aggregate sizes are given in Figure 8. Simulations on the two domain sizes are consistent showing good agreement in the region with overlap in terms of η_K / a.

Finally we analyse the impact of η_K / a on the morphology of the aggregates. The latter we quantify with their fractal dimension (symbol d_f). In our previous paper [13] we followed the common procedure for determining d_f based on plotting the radius of gyration (R_g) of a large collection of aggregates

versus the number of primary particles in the aggregate and fitting a power law $n_{agg} \propto R_g^{d_f}$ through the cloud of points. The width of the cloud and choices to be made in the fitting procedure make this quite an ambiguous exercise (see Figure 9). We settled [13] on a fitting procedure such that we only consider aggregates with size $n_{agg} \geq 4$, and force the fit through the a-priori known average radius of gyration of a sphere doublet (for $n_{agg} = 2$: $\frac{R_g}{a} = 1 + \frac{\delta}{\sqrt{3}a}$) so that only degree of freedom in the fit is d_f. This fit is given as the straight, solid line in Figure 9.

Figure 10 shows that the fractal dimension increases with increasing η_K / a. For the η_K / a ratios considered, the turbulent flow is unable to make dense aggregates; d_f does not exceed 1.8 (this value is reached for the highest η_K / a=0.361). These are fractal dimensions that are common for diffusion-limited aggregation [25]. Turbulent suspension flows with particles much smaller than the Kolmogorov length scale ($\eta_K / a \gg$) usually create more dense (higher d_f) aggregates [26]. We speculate that open aggregates with $\eta_K / a = O(0.1)$ – as we have here – the motion of primary particles is more erratic, i.e. diffusive.

5 Summary and conclusions

We have presented particle-resolved simulations of aggregating spheres in a fully resolved turbulent flow. The primary particle radius is larger than the Komogorov scale ($\eta_K / a < 1$) which makes the direct hydrodynamic environment of the particles inhomogeneous. The focus is on how turbulence interacts with the aggregation process. Turbulence plays a dual role: in the first place it promotes collisions that potentially lead to aggregation events, in the second place its fluid deformation induces disruptive forces on aggregates that can lead to breakage. At the same time, the presence of solids also couples back to the turbulence: the solid particles enhance small-scale turbulence, particularly in the moderately dense (solids volume fraction of the order of 0.1) suspensions studied here.

The turbulence is generated through linear forcing and is resolved down to the Kolmogorov scale. The square-well potential as aggregation mechanism was chosen for its simplicity. It only has two parameters and can be computationally efficiently combined with an event driven hard-sphere collision algorithm. We need the tight coupling between solid and fluid and the high level of detail including resolution of the flow around the particles since the Kolmogorov scale is of the same order of magnitude as the size of the primary particles and small-scale turbulence and the aggregation process have comparable and therefore interacting length scales. We clearly observed how stronger turbulence shifts aggregate size distributions towards smaller aggregates.

The aggregate structures were quantified by their fractal dimension d_f. Of large ensembles of aggregates, size n_{agg} and radius of gyration R_g were determined and the relationship $n_{agg} \sim \left(\frac{R_g}{a}\right)^{d_f}$ was fitted. This analysis showed wide scatter and related uncertainty in the fitting parameter d_f. Despite this uncertainty, it is clear that the aggregates have an open structure characterized by low fractal dimension: d_f did not exceed 1.8. We explain this by the erratic / diffusive nature of the particle motion in a turbulent field where particles are generally larger than the Kolmogorov scale.

The significance of the results presented in this paper mainly relates to the phenomenology of aggregation in turbulence. The abundant detail that is available from the simulations can be used to visualize and interpret the data from virtually any perspective. This helps in identifying trends and assessing the relative importance of competing physical mechanisms. Examples in this paper are the trends regarding η_K/a with an increase of (average) aggregate sizes *and* fractal dimension with increasing η_K/a.

At the same time, the conditions in the simulations are highly idealized (spherical particles, a simple interaction potential, homogeneous isotropic turbulence) making the road towards simulating real, physical, and practically relevant systems far from trivial. Further research could focus on (step-by-step) adding complication to the simulations, the first candidate being a more physically realistic interaction

potential / attractive force between particles. Validation through designing idealized physical experiments is a desirable future research direction as well.

References

[1] Ramkrishna, D.: Population balances – Theory and applications to particulate systems in engineering. Academic Press, London (2000).

[2] Marchisio, D.L., Pikturna, J.T., Fox, R.O., Vigil, D., Barresi, A.A.: Quadrature method of moments for population balances. AIChE J. 49, 1266-1276 (2003).

[3] Aamir, E., Nagy, Z.K., Rielly, C.D., Kleinert, T., Judat, B.: Combined quadrature method of moments and method of characteristics approach for efficient solution of population balance models for dynamic modeling and crystal size distribution control of crystallization processes. Ind. Eng. Chem. Res. 48, 8575-8584 (2009).

[4] Vigil, R.D.: On equilibrium slutions of aggregation-fragmentation problems. J. Colloid Interface Sc. 336, 642-647 (2009).

[5] Eggersdorfer, M.L., Kadau, D., Herrmann, H.J., Pratsinis, S.E.: Fragmentation and restructuring of soft-agglomerates under shear. J. Colloid Interface Sc. 342, 261-268 (2010).

[6] Bäbler, M.U., Morbidelli, M., Bałdyga, J.: Modelling the breakup of solid aggregates in turbulent flows. J. Fluid Mech. 612, 261-289 (2008).

[7] Zaccone, A., Soos, M., Lattuada, M., Wu, H., Bäbler, M.U., Morbidelli, M.: Breakup of dense colloidal aggregates under hydrodynamic stresses. Phys. Rev. E 79, 061401 (2009).

[8] Soos, M., Ehrl, L., Bäbler, M.U., Morbidelli, M.: Aggregate breakup in a contracting nozzle. Langmuir 26, 10-18 (2010).

[9] Higashitani, K., Iimura, K., Sanda, H.: Simulation of deformation and breakup of large aggregates in flows of viscous fluids. Chem. Engng. Sc. 56, 2927-2938 (2001).

[10] Becker, V., Schlauch, E., Behr, M., Briesen, H.: Restructuring of colloidal aggregates in shear flows and limitations of the free-draining approximation. J. Colloid Interface Sc. 339, 362-372 (2009).

[11] Harshe, Y.M., Lattuada, M., Soos, M.: Experimental and modeling study of breakage and restructuring of open and dense colloidal aggregates. Langmuir 27, 5739–5752 (2011).

[12] Harada, S., Tanaka, R., Nogami, H., Sawada, M.: Dependence of fragmentation behavior of colloidal aggregates on their fractal structure. J. Colloid Interface Sci. 301, 123-129 (2006).

[13] Derksen, J.J.: Direct numerical simulations of aggregation of monosized spherical particles in homogeneous isotropic turbulence. AIChE J. 58, 2589-2600 (2012).

[14] Rosales, C., Meneveau, C.: Linear forcing in numerical simulations of isotropic turbulence: Physical space implementations and convergence properties. Phys. Fluids 17, 095106-1-8 (2005).

[15] Smith, S.W., Hall, C.K., Freeman, D.B.: Molecular dynamics for polymeric fluids using discontinuous potentials. J. Comp. Phys. 134, 16-30 (1997).

[16] Chen, S., Doolen, G.D.: Lattice Boltzmann method for fluid flows. Annu Rev Fluid Mech. 30, 329-364 (1989).

[17] Succi, S.: The lattice Boltzmann equation for fluid dynamics and beyond. Clarendon Press, Oxford (2001).

[18] Goldstein, D., Handler, R., Sirovich, L.: Modeling a no-slip flow boundary with an external force field. J Comp Phys. 105, 354-366 (1993).

[19] Derksen, J., Van den Akker, H.E.A.: Large-eddy simulations on the flow driven by a Rushton turbine. AIChE J. 45, 209-221 (1999).

[20] Yamamoto, Y., Potthoff, M., Tanaka, T., Kajishima, T., Tsuji, Y.: Large-eddy simulation of turbulent gas-particle flow in a vertical channel: effect of considering inter-particle collisions. J. Fluid Mech. 442, 303-334 (2001).

[21] Somers, J.A.: Direct simulation of fluid flow with cellular automata and the lattice-Boltzmann equation. Appl Sci Res. 51, 127-133 (1993).

[22] Derksen, J.J., Sundaresan, S.: Direct numerical simulations of dense suspensions: wave instabilities in liquid-fluidized beds. J. Fluid Mech. 587, 303-336 (2007).

[23] Ten Cate, A., Nieuwstad, C.H., Derksen, J.J., Van den Akker, H.E.A.: PIV experiments and lattice-Boltzmann simulations on a single sphere settling under gravity. Phys. Fluids 14, 4012-4025 (2002).

[24] Kim, S., Karrila, S.J.: Microhydrodynamics: Principles and selected applications. Butterworth-Heinemann, Boston (1991).

[25] Witten Jr, T.A., Sander, L.M.: Diffusion-limited aggregation, a kinetic critical phenomenon. Phys. Rev. Letters 47, 1400-1403 (1981).

[26] Ehrl, L., Soos, M., Wu, H., Morbidelli, M.: Effect of flow field heterogeneity in coagulators on aggregate size and structure. AIChE J. 56, 2573-2587 (2010).

Figure 1. Impressions of the base-case simulation. A: Single realization showing all spheres in the domain colored by the size of the aggregate they are part of (red: $n_{agg} < 4$; yellow: $4 \le n_{agg} < 7$; green: $7 \le n_{agg} < 10$; blue: $n_{agg} \ge 10$). B: The four biggest aggregates (red: $n_{agg} = 60$, yellow: $n_{agg} = 150$, green $n_{agg} = 65$, blue: $n_{agg} = 105$; the red aggregate connects through the periodic boundaries). C: Evolution of the largest (yellow) aggregate in panel B shortly before and after its formation; different colors are different aggregates.

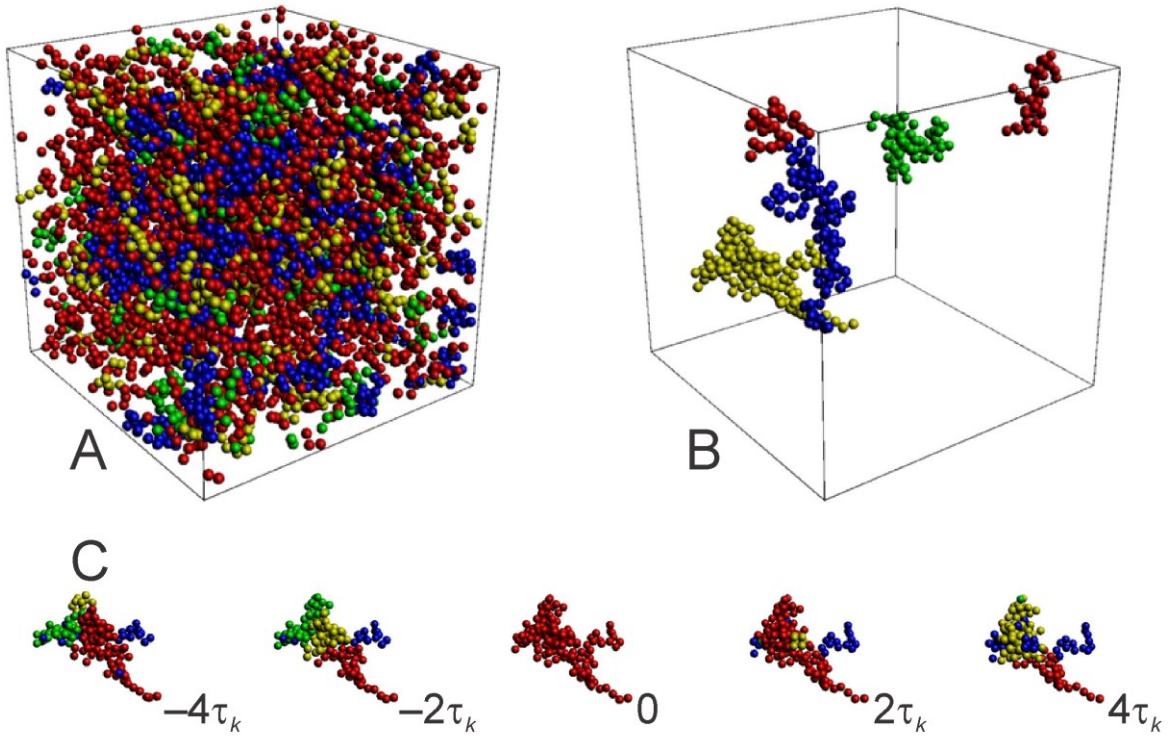

Figure 2. Top and middle: time series from a primary sphere perspective. Middle: size of an aggregate the primary sphere is part of. Top: absolute velocity of the primary sphere. The three colors are three different (randomly selected) spheres. Bottom: correlation of n_{agg} and $|\mathbf{v}_p|$ based on the time series. Base-case simulation.

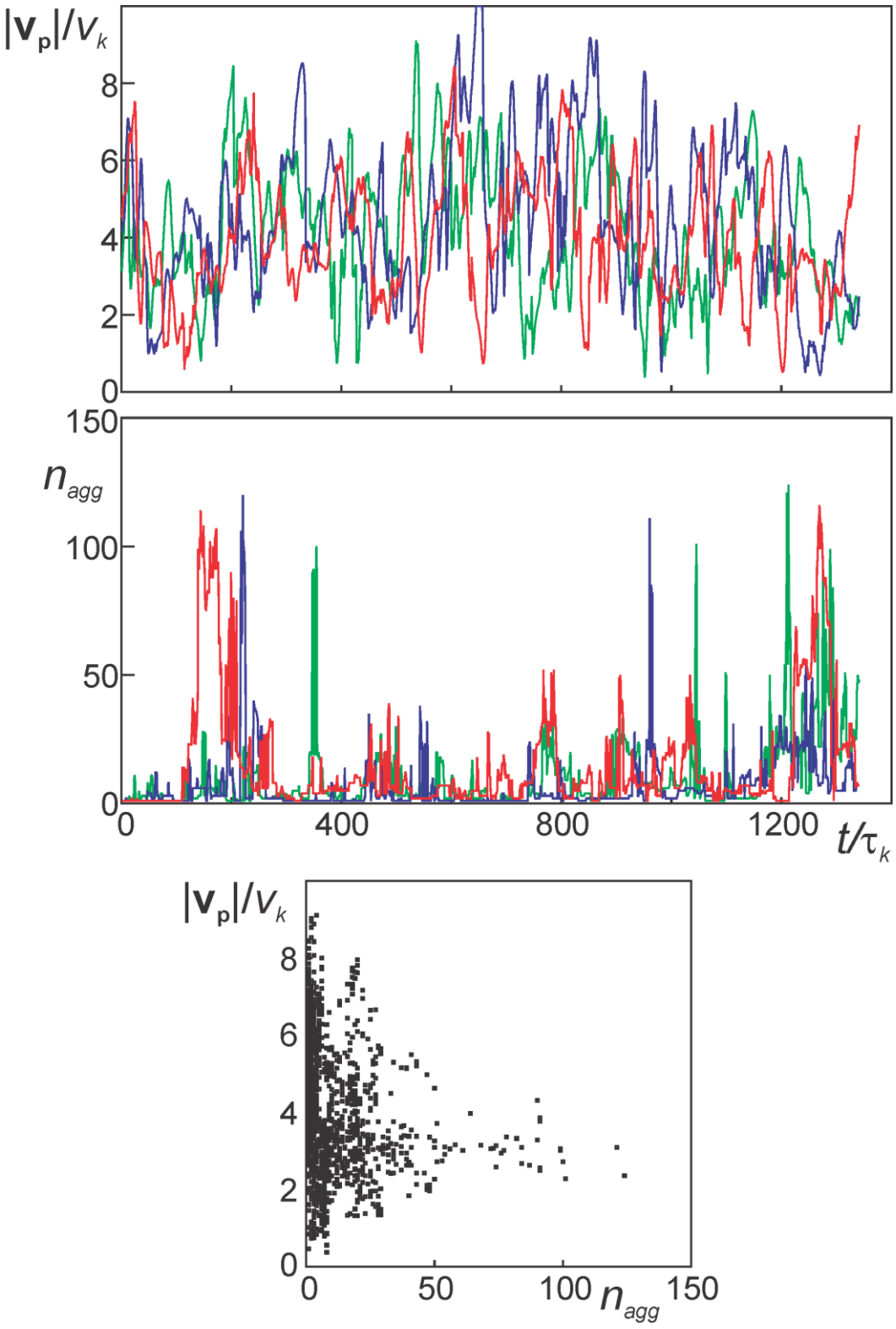

Figure 3. Left: primary particle velocity probability density functions (pdf's) for all particles and for particles with a specified number of contacts (n_c). Right: width of the pdf's as a function of n_c . Base-case conditions. Time averaging over a time window of $15a^2/\nu$ after steady state was reached.

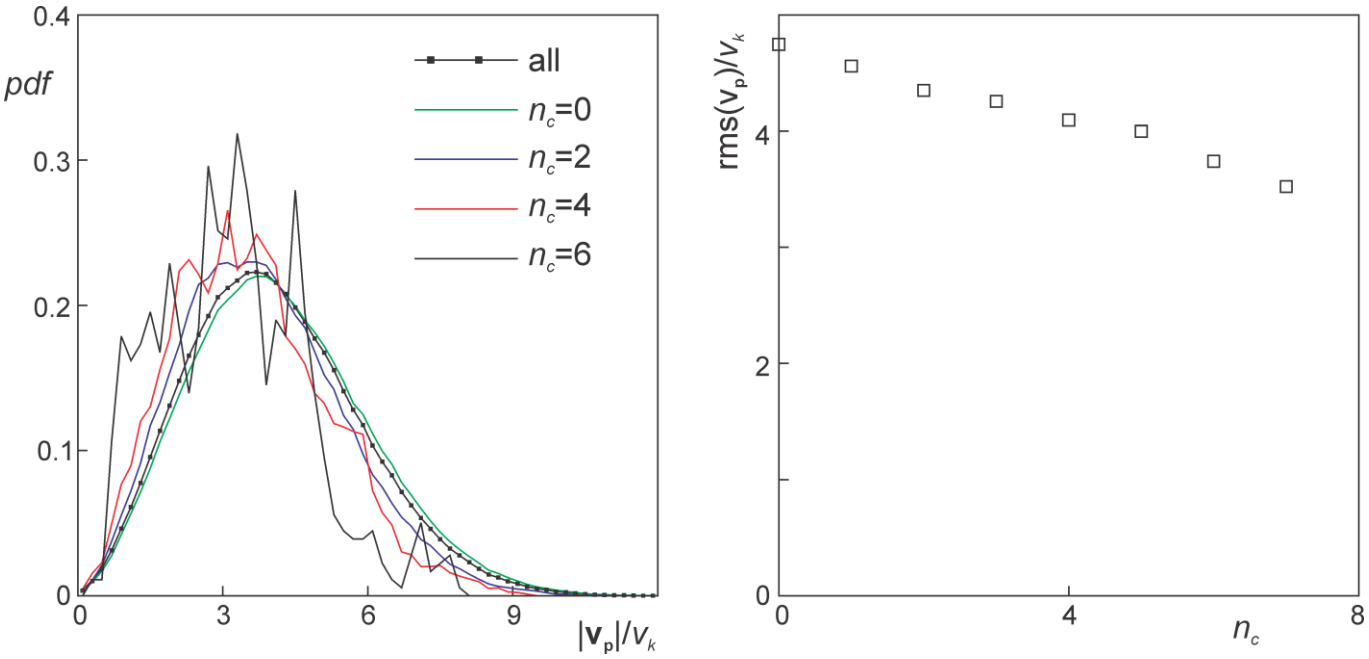

Figure 4. The average size of the aggregate a primary sphere having n_c contacting spheres is part of. Base-case conditions. Time averaging over a time window of $15a^2/\nu$ after steady state was reached.

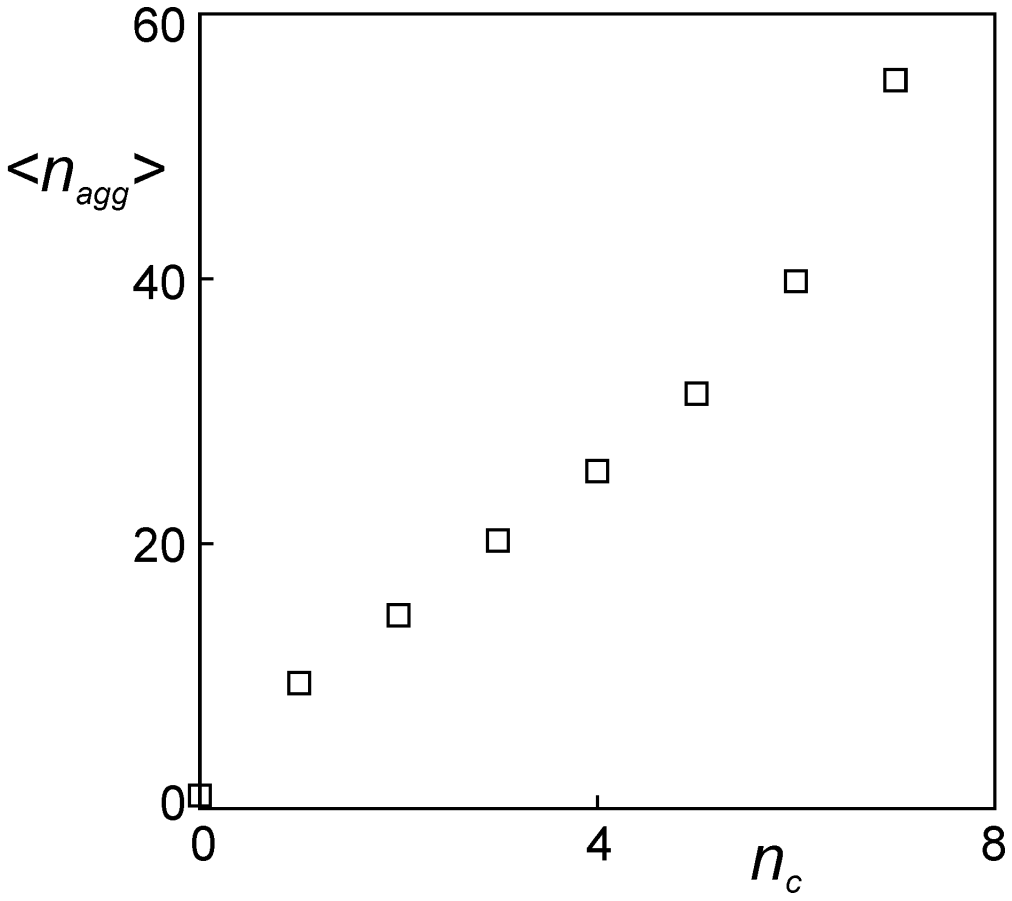

Figure 5. Aggregate size distributions by mass for the base-case (that has $\mu \to \infty$) and a case with the same conditions excepts that $\mu =$.

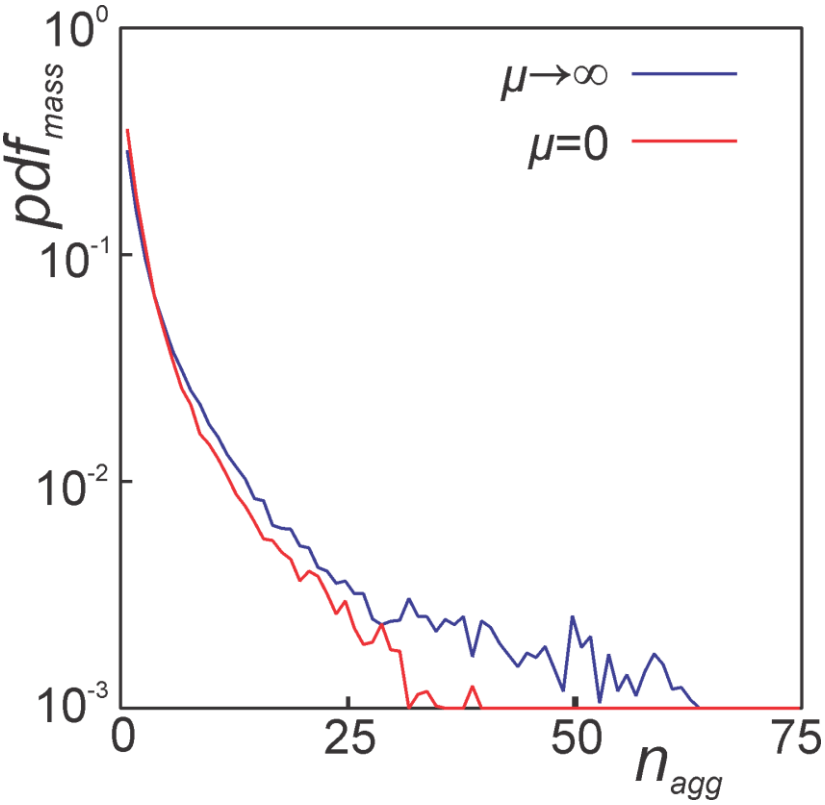

Figure 6. ASDs by mass for L=256 (left) and 384 (right) domains, effect of $\left\langle \frac{\eta_K}{a} \right\rangle$. Time averaging over a time window of $15a^2/\nu$ (for L=256) and $4.7a^2/\nu$ (L=384) after steady state was reached.

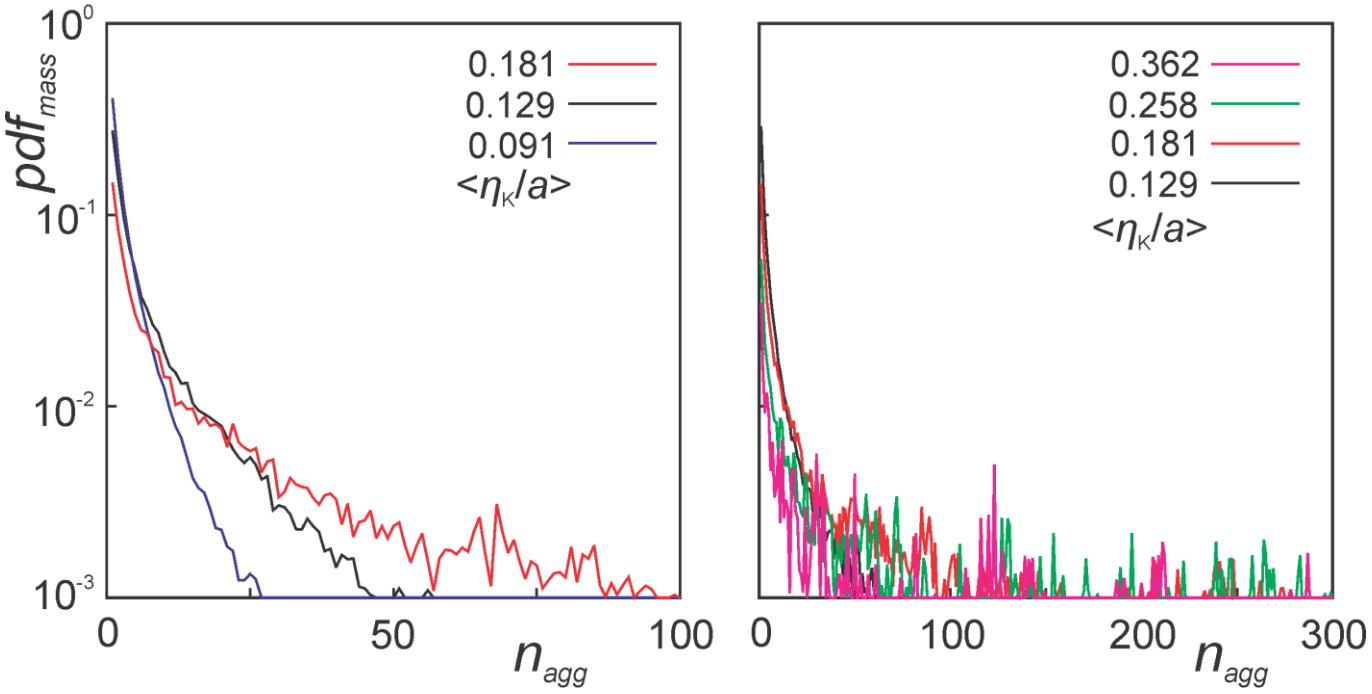

Figure 7. Average particle-based Reynolds number $\mathrm{Re}_{rms,a} \equiv \frac{u_{rms} a}{\nu}$ as a function of $\left\langle \frac{\eta_K}{a} \right\rangle$ for two different domain sizes (as indicated). Base case conditions.

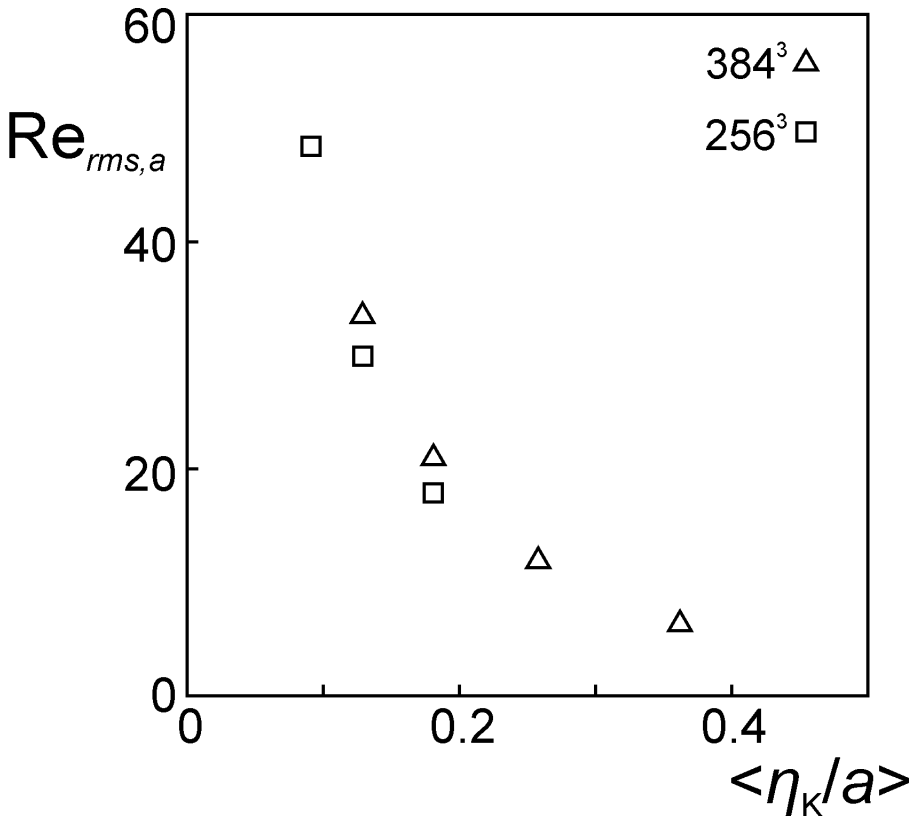

Figure 8. Average agglomerate size as a function of $\langle \eta_K / a \rangle$. Results for two different domain sizes as indicated. Base-case conditions except for $\langle \eta_K / a \rangle$.

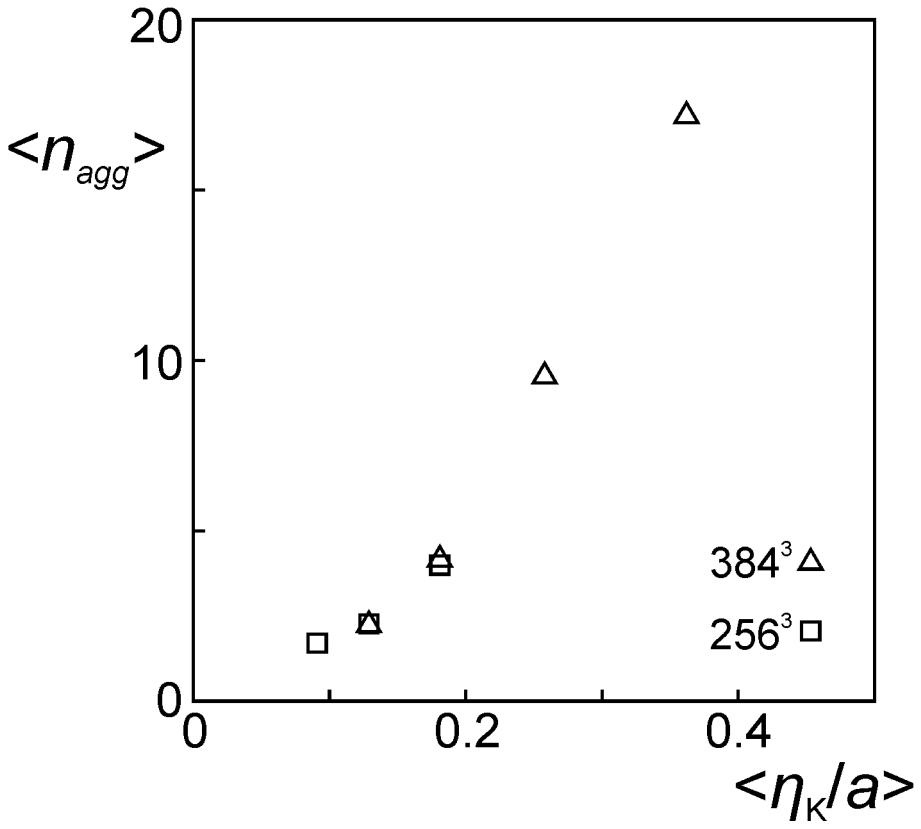

Figure 9. Radius of gyration $\frac{R_g}{a}$ versus aggregate size n_{agg}. Base-case. Dots: individual aggregates. Red line: fit according to $n_{agg} \propto R_g^{df}$ with d_f the fractal dimension and only degree of freedom in the fit (see text for details). The fit only considers aggregates with $n_{agg} \geq 4$.

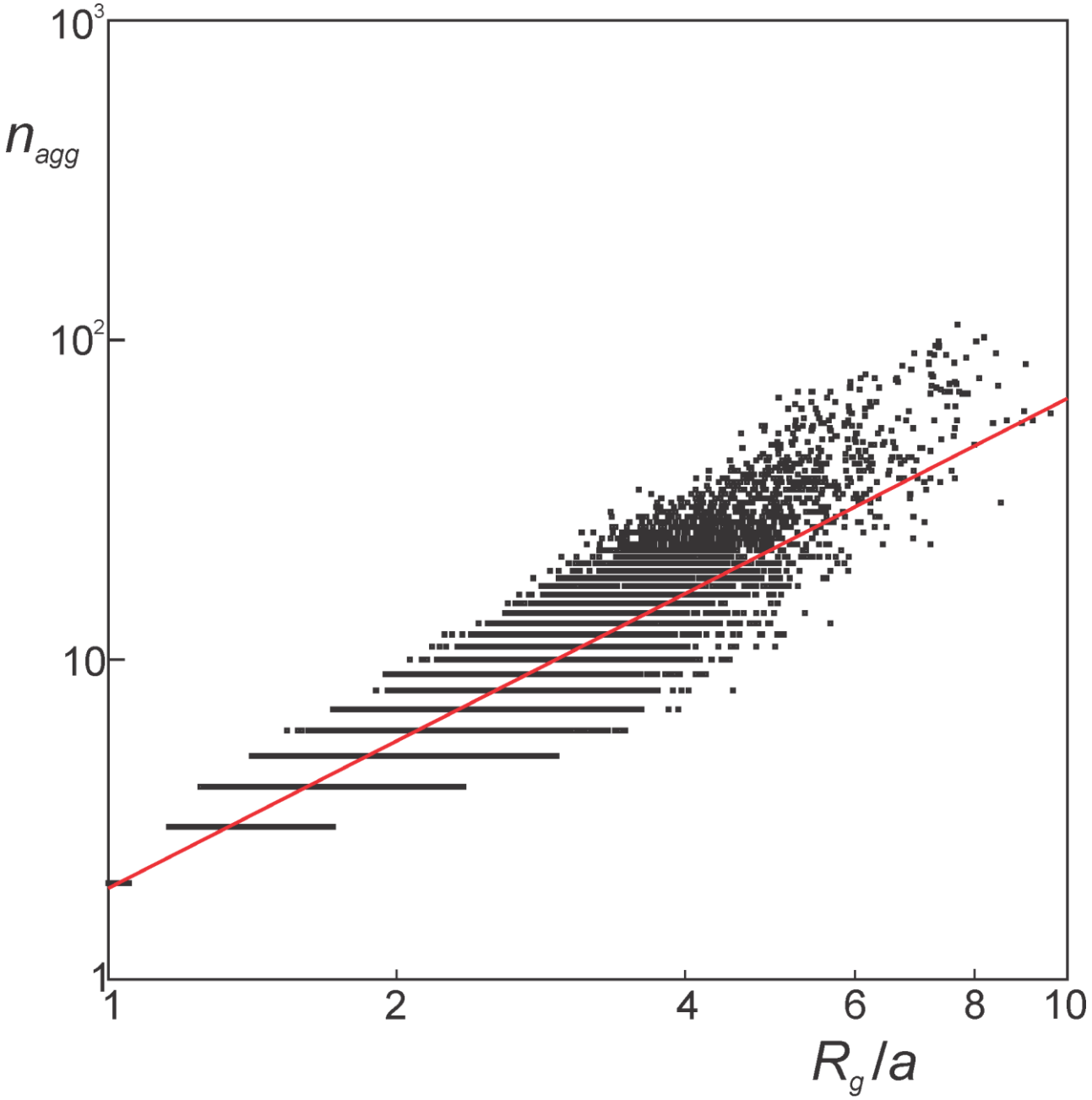

Figure 10. Fractal dimension as a function of $\langle \eta_K / a \rangle$. Results for two different domain sizes as indicated. Base-case conditions except for $\langle \eta_K / a \rangle$.

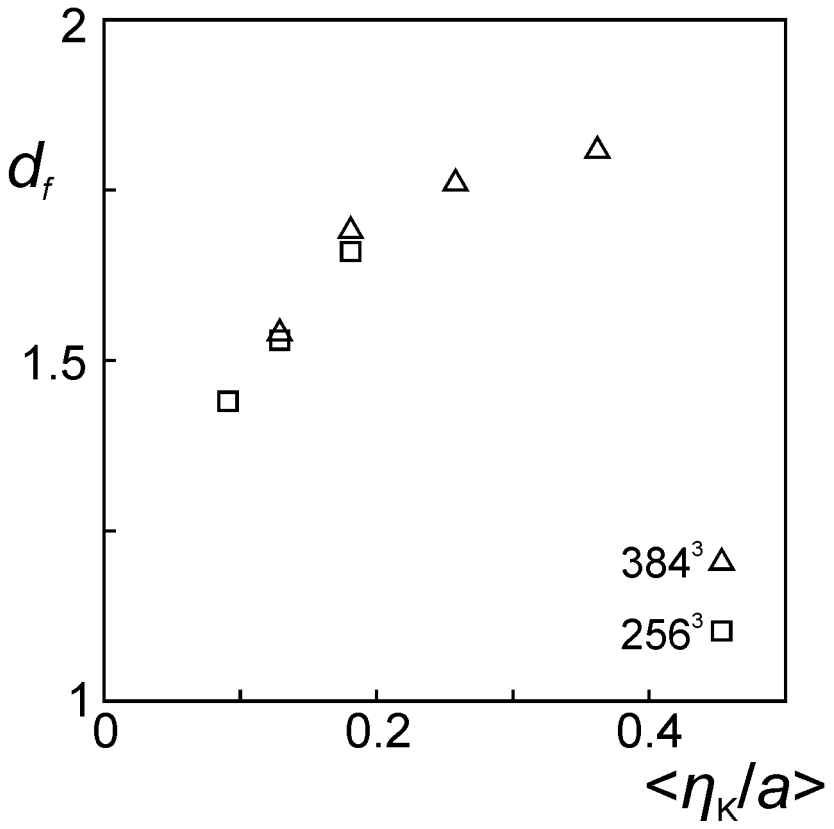

Table 1. *Base-case input settings.*

$\frac{\rho_p}{\rho}$	ϕ	$\frac{\eta_K}{a}$	$\frac{\delta}{a}$	$\frac{\Delta u}{\upsilon}$	e	μ
4.0	0.08	0.129	0.05	0.30	1.0	∞